

Voyaging into Unbounded Dynamic Scenes from a Single View

Fengrui Tian Tianjiao Ding Jinqi Luo Hancheng Min René Vidal
University of Pennsylvania

{tianfr,tjding,jinqiluo,hanchmin,vidalr}@seas.upenn.edu

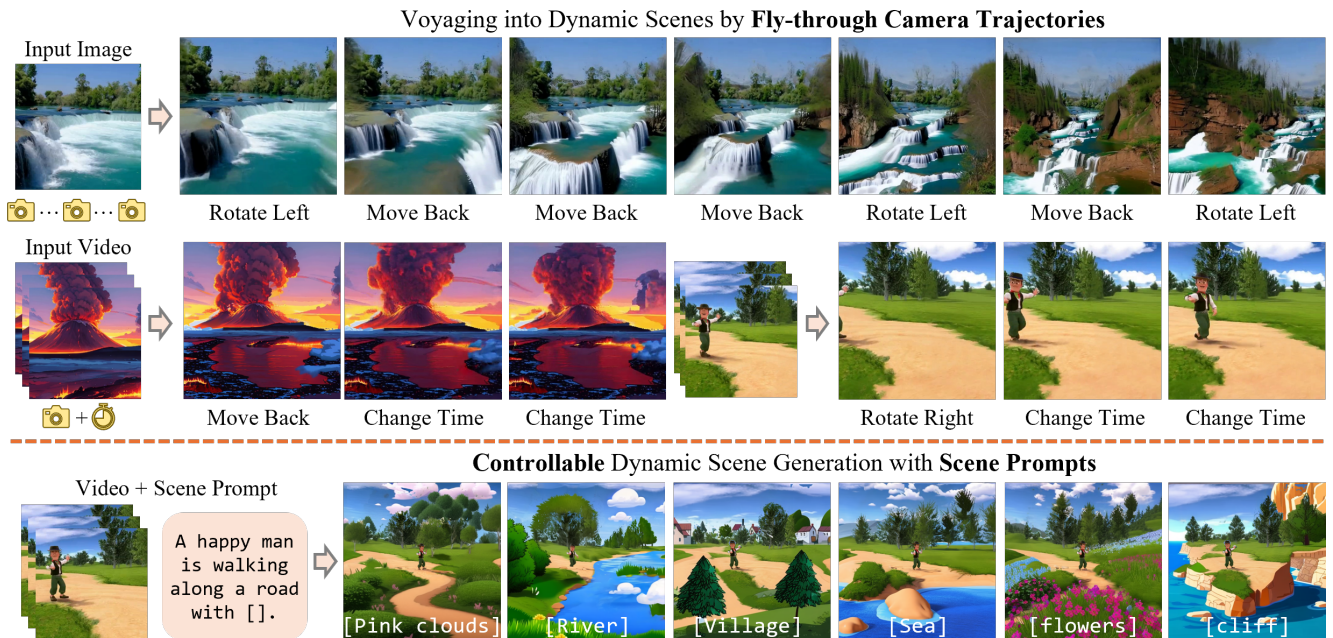


Figure 1. DynamicVoyager generates 4D point clouds of unbounded dynamic scenes by our dynamic scene outpainting process. Given a fixed viewpoint video (or an image with a motion prompt) with dynamic scene prompts and fly-through camera trajectories, DynamicVoyager can generate dynamic scenes along the trajectories (**Top**) and control scene generation contents (**Bottom**).

Abstract

This paper studies the problem of generating an unbounded dynamic scene from a single view, which has wide applications in augmented/virtual reality and robotics. Since the scene is changing over time, different generated views need to be consistent with the underlying 3D motions. While previous works learn such consistency by training from multiple views, the generated scene regions are bounded to be close to the training views with limited camera movements. To address this issue, we propose DynamicVoyager that reformulates the dynamic scene generation as a scene outpainting process for new dynamic content. As 2D outpainting models can hardly generate 3D consistent motions from only 2D pixels at a single view, we consider **pixels as rays** to enrich the pixel input with the ray context, so that the 3D

motion consistency can be learned from the ray information. More specifically, we first map the single-view video input to a dynamic point cloud with the estimated video depths. Then we render the partial video at a novel view and outpaint the video with ray contexts from the point cloud to generate 3D consistent motions. We employ the outpainted video to update the point cloud, which is used for scene outpainting from future novel views. Experiments show that our model is able to generate unbounded scenes with consistent motions along fly-through cameras, and the generated contents can be controlled with scene prompts.

1. Introduction

Scene generation [31, 57, 58] aims to create a virtual scene with 3D representations such as point clouds [17, 57],

meshes [8], neural radiance fields [32, 43] and 3D Gaussians [21]. It has many applications in augmented reality (AR), virtual reality (VR) [4, 5] and robotics [9]. While recent studies have achieved significant progress in generating a static scene [27, 57, 58] from a single image by leveraging the power of diffusion models [3, 41], these approaches cannot generate scenes with vivid dynamic contents, which fail to meet downstream needs. For example, AR/VR game designers need to build a dynamic scene for the players to explore and interact. Likewise, robotics researchers often require a virtual scene containing commonly seen dynamic objects in natural environments for self-exploration embodied agents [11, 52].

Generating dynamic scenes from a single view is a challenging task. The generated dynamic contents (*e.g.*, hands waving, rivers flowing) need to maintain 3D consistency: when we observe the generated dynamic scenes from two different views, the observed motions should have 3D correspondence between those two views. As we can only observe 2D motions on the image plane from the 2D image pixels at one single view, there is a 2D-to-3D ambiguity when generating 3D consistent motions at a novel view from these pixels. Previous works [26, 28, 42, 50, 56] address this challenge by learning from multiple views surrounding the dynamic scenes, so that the 3D motion information can be implicitly learned from the 2D motions observed in these views.

However, while these scene generation models trained on surrounding views successfully generate consistent 3D motions, the generated dynamic regions are strictly bounded by the input views with a limited range of camera motions, as exemplified in Figure 2. Such limitation severely restrains the models from creating unbounded dynamic scenes, which have an increasing demand in AR/VR and robotics. This further limits the development of controllable scene generation with human guidance. A natural question is raised: can we generate an unbounded dynamic scene from a single view?

In this paper, we provide a positive answer to this question. We present DynamicVoyager, which reformulates dynamic scene generation as a scene outpainting process, enabling the creation of new dynamic content in the unseen areas. In this way, our generated scenes can be explored from a single view to any place with fly-through camera trajectories. Note that traditional 2D outpainting models can hardly generate 3D consistent object motions by only leveraging 2D image pixel input at a single view, as 2D pixels in consecutive frames contain limited 3D motion information. To address this, we consider *pixels as rays* to enrich the pixel input with the context of camera rays, so that the 3D motion information can be learned from the ray context information in the 3D space.

More specifically, for an image input, we exploit image-



Figure 2. Failure examples of previous dynamic scene generation methods. While the generated dynamic scenes from previous works [42, 49, 50] are strictly bounded by the input views, DynamicVoyager successfully generates dynamic scenes with large camera motions by the proposed scene outpainting process.

to-video diffusion models [16, 54] to synthesize a fixed pose video from that image. Then for the video input, we first estimate the video depth maps and backproject the fixed view-point video frames into 3D space as dynamic point clouds with the estimated depths. After that, we render a partial video from the reconstructed point clouds at a novel view. By viewing pixels as rays, we sample ray depth maps of overlapping regions between two views, and compute the distance between rays and the point clouds as complementary 3D information for the unseen areas. This allows us to outpaint the unseen regions in the partial video with the sampled ray depths and ray distance maps to generate 3D consistent motions. Finally, we estimate the depth maps of the outpainted video and update the unseen regions of the dynamic point clouds. Figure 1 visualizes examples of dynamic scenes generated by our method using input from a video with a fixed camera pose or a single image. Experiments demonstrate that our model effectively generates unbounded dynamic scenes with 3D consistent motions along fly-through camera trajectories and controls the outpainting with scene prompts.

2. Related Work

Static scene generation. With the development of vision foundation models [20, 22, 37, 40, 47], many works have started to generate static scenes from input images [2, 7, 10] or text prompts [15, 31]. Early efforts focused on indoor scene generation [2, 7, 15, 25] or object-centric scene generation [10]. These methods firstly generate multiview images of the target scene and fuse the multiview images by using 3DGS [21] or NeRF [32, 43, 44] representations. However, they can only generate static scenes with limited ranges of camera motions. When the camera moves drastically, these methods fail to generate unseen regions with consistent and clear scene structures. To overcome this issue, later studies have started to explore *perpetual view generation* [30] that allows larger camera movements [19, 27, 30, 35, 57, 58]. Notably, WonderJourney [58] and WonderWorld [57] propose to generate an infinite world with diverse contents by using a combination of state-of-the-art depth estimation

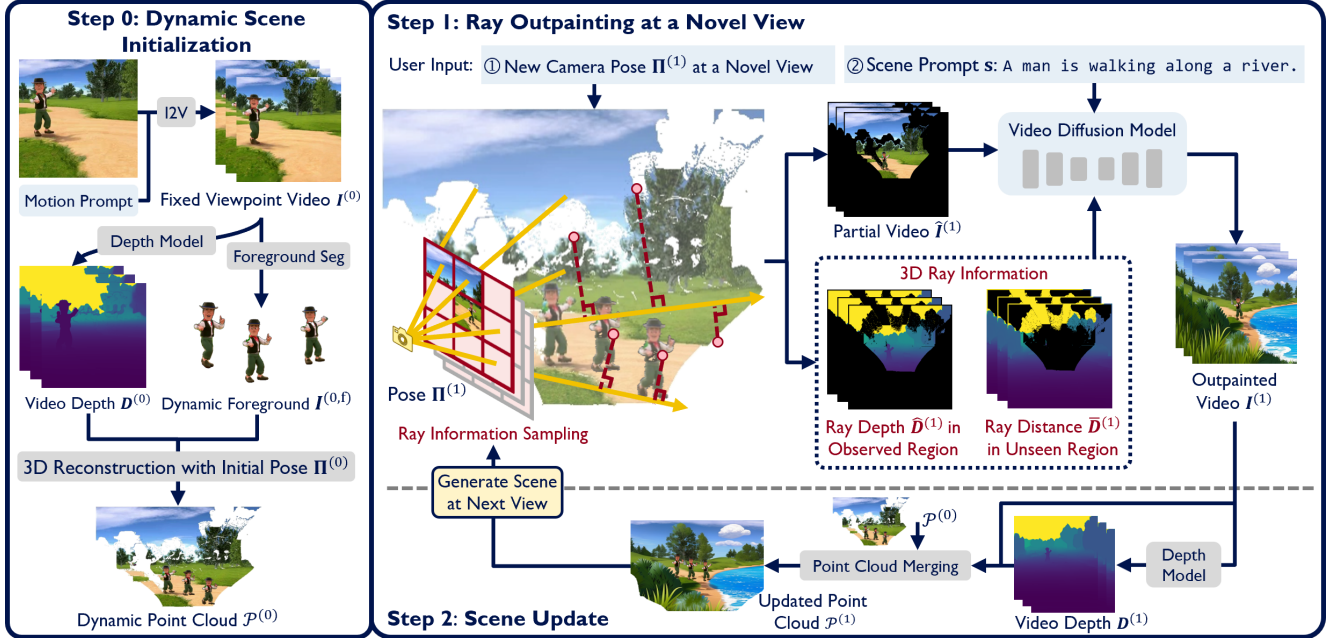


Figure 3. The overview of DynamicVoyager. First, for an initial camera pose, we build the dynamic point clouds from the input image by employing the image-to-video diffusion model [54], depth model [37] and foreground segmentation model [20] (§3.1). Then given a new camera pose, we render the partial video and the corresponding ray depth and ray distance maps. We consider pixels as rays to enrich the pixel information of the partial video with the corresponding ray depth and ray distance information for outpainting the video with consistent motions (§3.2). Finally, we update the dynamic point cloud with the outpainted video and the corresponding video depth (§3.3).

[37], image segmentation [22] and object detection models [20]. However, these methods can only generate diverse scenes with static objects. In this paper, we target the problem of generating dynamic scenes with new dynamic contents with fly-through camera trajectories.

Dynamic scene generation. Following the great success of static scene generation methods, recent studies have started to address the dynamic scene generation problem [26, 28, 34, 38, 42, 49, 50, 55, 56]. Due to the limited resources of real-world dynamic scene data, many researchers try to leverage the pretrained video diffusion models [16, 39, 51, 54] to generate multiple views of dynamic scenes. A key challenge in this setting is maintaining 3D motion consistency in multiple generated views. CAT4D [49] and DimensionX [42] learn to generate 3D consistent motion from multiview datasets [6, 29]. However, as the multiview images in these datasets are taken from cameras that are very close to each other, the generated dynamic scenes in these methods are strictly limited by the input images or videos. 4K4DGen [26] animates 3D consistent motion by building a 3D consistent noise space in the diffusion models. GEN3C [39] achieves camera control of dynamic scenes with 4D point cloud representations. However, since these methods only interpolate novel views surrounding the input image or videos, they still cannot generate new dynamic contents in the unseen regions of the input images.

In this paper, we consider dynamic scene generation as a scene outpainting problem so that our method can generate new dynamic content with fly-through camera motions in the unseen regions of the input video.

Video diffusion models. Our method relies on the power of the recent video diffusion models [51, 54] to outpaint dynamic scenes with diverse contents. While some researchers propose video diffusion models with controllable camera trajectories [1, 12, 13, 17, 24, 45, 53, 60], these trajectories are bounded by the regions of the input views (a failure case is shown in Figure 8). Besides, since the outputs of these methods are generated videos without any 4D scene structures, they always encounter view inconsistency issues when fusing 4D representation with the output videos. Instead, our method adopts 4D point clouds as the dynamic scene representation and outpaints the dynamic point clouds with video outpainting models, where the unseen regions in the input video can be generated by the outpainting procedure, and the motion consistency in different views can be achieved by introducing ray information in 3D space.

3. Approach

In this section, we propose DynamicVoyager for generating unbounded dynamic scenes, which includes three steps as summarized in Figure 3 and below.

- (§3.1 Dynamic Scene Initialization) DynamicVoyager accepts either a video with a fixed camera pose or an image with a prompt describing object motions; in the latter case, it first generates a video with a fixed pose. A depth map is then estimated from each frame of the video. We segment the video into a dynamic foreground and a static background, reconstruct the point clouds separately, and aggregate these into one dynamic point cloud.
- (§3.2 Ray Outpainting) At a new given pose, the goal is to generate a video consistent with the existing dynamic point cloud and a given scene prompt. We first rasterize the point cloud at the new pose, which is consistent by construction. That said, the rasterization only fills in part of the image, so the question is how to outpaint the rest *consistently*. To do so, we propose to guide the outpainting process with 3D information by providing the model with ray depth in the observed region and the distance of rays to the point cloud in the unseen region.
- (§3.3 Dynamic Scene Update) We update the dynamic point cloud via the video from the new pose. We repeat §3.2 and §3.3 to iteratively update the dynamic point cloud from novel poses.

3.1. Dynamic Scene Initialization

We begin by describing how to generate an initial dynamic point cloud given a video at a fixed camera pose $\Pi^{(0)}$ or an image with a motion prompt. Notation-wise, a superscript (i) denotes objects related to the i^{th} camera pose $\Pi^{(i)}$.

For illustration, suppose we are given an image $I_0^{(0)} \in \mathbb{R}^{h \times w \times 3}$, where $h, w, 3$ are respectively height, width and number of color channels, as well as a prompt describing the desired motion for the video. To generate a video at the fixed pose $\Pi^{(0)}$, we employ a pretrained image-to-video diffusion model [54] by providing both $I_0^{(0)}$ and the motion prompt, where the motion prompt is further prepended with Camera is strictly fixed. We let $I^{(0)} = \{I_t^{(0)}\}_{t=0}^{N-1}$ denote the generated video, where $I_t^{(0)}$ denotes its t^{th} frame.

Given the generated or user-input fixed viewpoint video $I^{(0)}$, we reconstruct the underlying dynamic scene, represented as 4D point cloud $\mathcal{P}^{(0)} = \{\mathbf{p} = (\mathbf{x}, t, \mathbf{c})\}$, where $\mathbf{x} \in \mathbb{R}^3$, $t \in \mathbb{R}$ and $\mathbf{c} \in \mathbb{R}^3$ denote the 3D position, timestamp and color respectively. Since the objects in the video foreground and the scene in the background have different dynamic natures, our framework reconstructs point cloud $\mathcal{P}^{(0,f)}$ for the foreground scene and $\mathcal{P}^{(0,b)}$ for background separately. To this end, we extract the binary video foreground masks $M^{(0)} = \{M_t^{(0)} \in \{0, 1\}^{h \times w}\}_{t=0}^{N-1}$ with the foreground segmentation method [20] to segment the video $I^{(0)}$ into foreground video $I^{(0,f)} = \{I_t^{(0,f)}\}_{t=0}^{N-1}$ and background video $I^{(0,b)} = \{I_t^{(0,b)}\}_{t=0}^{N-1}$. We employ the depth model [37] on video $I^{(0)}$ to obtain the video depth maps $D^{(0)} = \{D_t^{(0)} \in \mathbb{R}^{h \times w}\}_{t=0}^{N-1}$. Next, we describe the fore-



Figure 4. Qualitative ablation studies of the proposed foreground layer (§3.1) and background completion (§3.3) strategy.

ground and background scene initialization steps.

Scene foreground initialization. We exploit the depth maps $D^{(0)}$ and foreground masks $M^{(0)}$ to obtain the foreground depth maps $D^{(0,f)} = \{D_t^{(0,f)}\}_{t=0}^{N-1}$. Since the video is captured with a fixed camera, we initialize the video camera pose $\Pi^{(0)}$ as the center of the dynamic scene. We reconstruct the initial foreground point cloud by employing the foreground video frames $I^{(0,f)}$, foreground depth maps $D^{(0,f)}$ and the initial camera pose $\Pi^{(0)}$,

$$\mathcal{P}_t^{(0,f)} = \phi([I_t^{(0,f)}, D_t^{(0,f)}], \Pi^{(0)}, t), t \in \{0, \dots, N-1\}, \quad (1)$$

where $\mathcal{P}_t^{(0,f)}$ denotes the foreground point cloud at timestamp t . ϕ denotes the mapping from an image with its depth map to the point cloud. We obtain the foreground point cloud at all timestamps $\mathcal{P}^{(0,f)} = \bigcup_{t=0}^{N-1} \mathcal{P}_t^{(0,f)}$.

Scene background initialization. Since the backgrounds do not have motions in the dynamic scene, we hypothesize that the pixel at the same location on the different video frames has the same 3D position at different timestamps. More specifically, let $D_t^{(0)}(x, y)$, $M_t^{(0)}(x, y)$ denote the depth and foreground mask values at x^{th} row and y^{th} column of the video frame $I_t^{(0)}$. The background depth can be element-wise calculated by the following equation,

$$D^{(0,b)}(x, y) = \frac{\sum_{t=0}^{N-1} D_t^{(0)}(x, y) \cdot (1 - M_t^{(0)}(x, y))}{\sum_{t=0}^{N-1} (1 - M_t^{(0)}(x, y))}, \quad (2)$$

where $D^{(0,b)}$ is the refined background depth map. We employ the same mapping function ϕ to map the background regions on the video frames to the 4D point clouds,

$$\mathcal{P}_t^{(0,b)} = \phi([I_t^{(0,b)}, D^{(0,b)}], \Pi^{(0)}, t), t \in \{0, \dots, N-1\}. \quad (3)$$

In this way, the obtained background point clouds $\mathcal{P}^{(0,b)} = \bigcup_{t=0}^{N-1} \mathcal{P}_t^{(0,b)}$ have time-invariant positions and time-varying colors. Finally, we obtain the scene point cloud by merging the foreground and background point clouds,

$$\mathcal{P}^{(0)} = \mathcal{P}^{(0,f)} \cup \mathcal{P}^{(0,b)}, \quad (4)$$

which is then introduced for outpainting the scene at a novel view with 3D consistent motions.

3.2. Ray Outpainting at a Novel View

We now need to outpaint the scene at a given novel pose $\Pi^{(1)}$. We follow the assumption of previous works [23, 57, 58] that the view of $\Pi^{(1)}$ overlaps moderately with that of $\Pi^{(0)}$ to allow for outpainting a substantial portion of the scene. The question is, how can we outpaint a dynamic scene containing consistent motions with the existing dynamic point cloud $\mathcal{P}^{(0)}$?

We first rasterize the point cloud at $\Pi^{(1)}$, so that the observed region in the resulting partial video has obviously consistent motions with the point cloud. To handle the unseen region, a naive proposal is to directly outpaint the partial video. However, this typically leads to inconsistencies across the boundary of observed and unseen regions, as we visualize in Figure 5. Our intuition is that pixels in each video frame only provide 2D information which is not enough to reconstruct the 3D motion. Therefore, we consider pixels as rays: during the rasterization, we save the ray depth map aligned with each pixel to provide 3D ray information in the observed region; in the unseen region, we compute the distance between the rays (from the camera origin through the pixels) and the point cloud, to serve as guidance on how much the generated pixel should respect the existing point cloud.

Ray information sampling at the observed regions.

Given a novel pose $\Pi^{(1)}$, we first rasterize the dynamic point cloud $\mathcal{P}^{(0)}$: for every time $t \in \{0, \dots, N-1\}$, we do

$$(\hat{\mathbf{I}}_t^{(1)}, \hat{\mathbf{D}}_t^{(1)}, \hat{\mathbf{M}}_t^{(1)}) = \varphi(\mathcal{P}_t^{(0)}, \Pi^{(1)}). \quad (5)$$

Here, φ denotes the image rasterization function. $\hat{\mathbf{M}}_t^{(1)}$ is a binary mask where $\hat{\mathbf{M}}_t^{(1)}(x, y) = 1$ if at least one 3D point from $\mathcal{P}_t^{(0)}$ hits the image pixel at the x^{th} row and y^{th} column during rasterization and 0 otherwise. Correspondingly, $\hat{\mathbf{I}}_t^{(1)}$ is the rasterized partial video and $\hat{\mathbf{D}}_t^{(1)}$ the rasterized *ray depth* map (to be distinguished from the depth map generated by depth models as in §3.1). A hat on the notation emphasizes that the signals are not observed for all locations, and we denote $\hat{\mathbf{D}}^{(1)} = \{\hat{\mathbf{D}}_t^{(1)}\}_{t=0}^{N-1}$, $\hat{\mathbf{M}}^{(1)} = \{\hat{\mathbf{M}}_t^{(1)}\}_{t=0}^{N-1}$ and $\hat{\mathbf{I}}^{(1)} = \{\hat{\mathbf{I}}_t^{(1)}\}_{t=0}^{N-1}$. A few remarks are in order. First, by doing the rasterization, the observed regions are obviously consistent with the point cloud. Moreover, the ray depth maps encode the 3D information of the observed scene, which as we shall see will be included as guidance for outpainting. For the regions not observed at $\Pi^{(1)}$, we introduce the distance between rays and the point cloud in the following to complement the 3D information in these regions.

Ray-point-cloud distance computation in unseen region.

Fix the reference coordinate system at the origin of a camera. Let $\mathbf{r} \in \mathbb{R}^3$ be a unit vector denoting the direction of a ray from the origin pointing at a pixel location, and $\mathbf{p} \in \mathbb{R}^3$

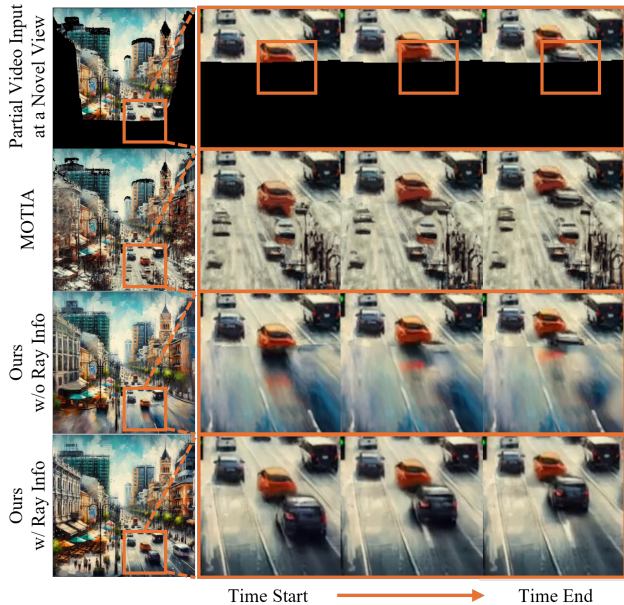


Figure 5. Ablation studies of scene outpainting with ray information. We also compare with the 2D outpainting model MOTIA [46]. Detailed visualization demonstrates that with ray information, our model successfully outpaints the dynamic scenes with consistent motions.

a point in the 3D space. We recall that the distance between the ray and the 3D point can be computed as

$$\text{dist}_{\text{r2p}}(\mathbf{r}, \mathbf{p}) = \sqrt{\|\mathbf{p}\|_2^2 - (\mathbf{r}^\top \mathbf{p})^2}. \quad (6)$$

With the above said, we can compute the distance between camera rays and the 4D point cloud for the complementary 3D information of the unseen regions. Namely, we compute

$$\bar{\mathbf{D}}_t^{(1)}(x, y) = \min_{\mathbf{p} \in \mathcal{P}_t^{(0)}} \text{dist}_{\text{r2p}}(\mathbf{r}^{(1)}(x, y), \mathbf{p} - \mathbf{o}^{(1)}), \quad (7)$$

where $\mathbf{r}^{(1)}(x, y) \in \mathbb{R}^3$ is the unit-norm ray vector starting from the origin of $\Pi^{(1)}$ pointing at pixel (x, y) , and $\mathbf{o}^{(1)}$ is the camera center of $\Pi^{(1)}$, both in the reference coordinate system of $\Pi^{(0)}$. As we will see, such a distance will be used to guide the outpainting.

Ray outpainting. To outpaint the dynamic scene at the novel pose $\Pi^{(1)}$ from the partial video, we desire a few properties for the outpainted video: 1) the outpainted video needs to have a static pose fixed at $\Pi^{(1)}$ and be consistent with the existing dynamic point cloud in the observed region, 2) the user should be able to control the generation in the outpainted region (i.e., the unseen region), and 3) the motions in the outpainted region need to be consistent with the motions in the observed region. To fulfill properties 1) and 2), we design our video outpainting model to take as

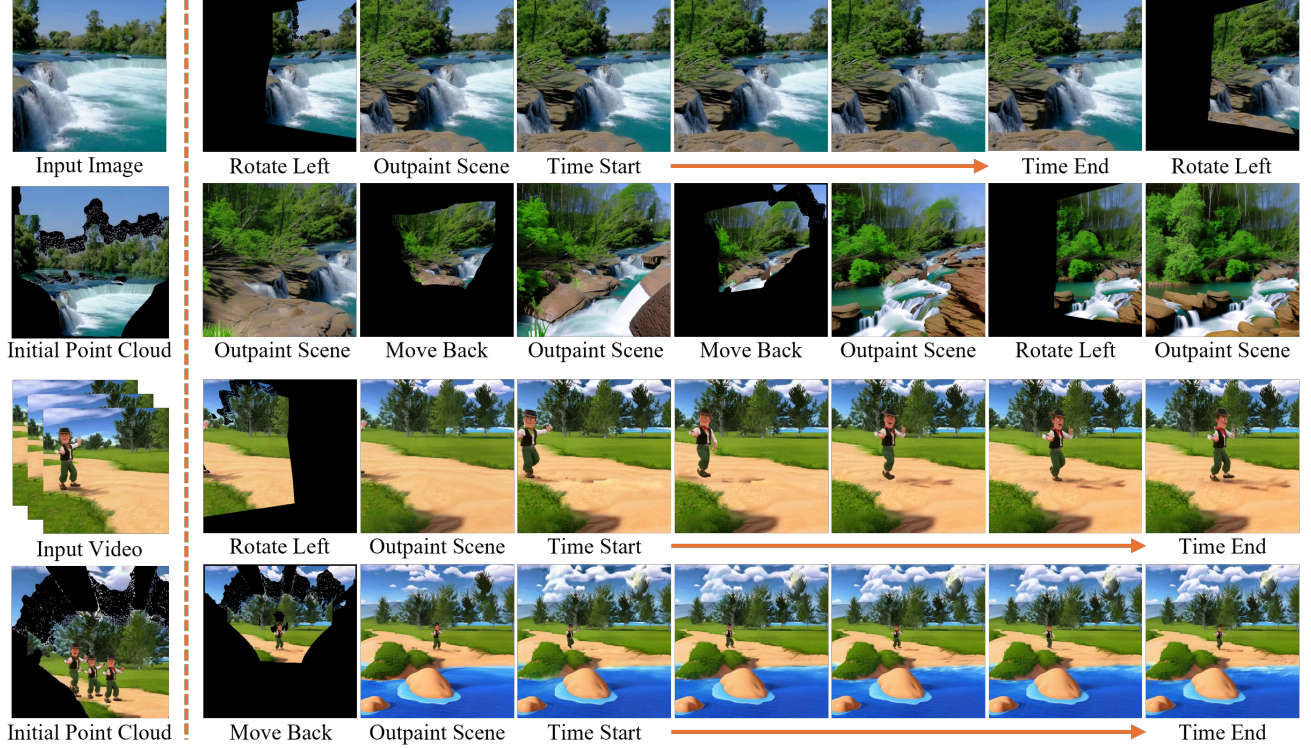


Figure 6. Voyaging into unbounded dynamic scenes with long camera trajectories from a single image or fixed viewpoint video. We iteratively show the unseen regions through large camera motions, the dynamic scene outpainting results and the consistent motions from novel views. By enriching the pixel information with ray contexts, our method successfully builds large dynamic scenes from input views.

input the extracted partial video $\hat{I}_t^{(1)}$, as well as a prompt narrating the desired motions in the generated scene. For property 3), we propose to employ ray depth map $\hat{D}^{(1)}$ and ray distance map $\bar{D}^{(1)}$ as guidance on 3D information in the observed region and how much the outpainted ray in the unseen region should respect the existing point cloud. To sum up, our video outpainting model accepts the partial video $\hat{I}^{(1)}$, scene prompt s , ray depth map $\hat{D}^{(1)}$, ray distance map $\bar{D}^{(1)}$ and generates an outpainted video $I^{(1)} = \{I_t^{(1)}\}_{t=0}^{N-1}$. Next we describe how to train such a video outpainting model.

Training outpainting model. As we need the ray information to train our video outpainting model, we extract depth maps of the training videos and initialize a camera with the same intrinsics of $\Pi^{(0)}$ to calculate the ray information. More specifically, given a training video I , we extract the video depth maps D with the depth model [37]. We apply a random video mask to the video and the depth maps to generate partial video \hat{I} and partial depth maps \hat{D} . Then we initialize a fixed camera pose Π at the world center whose intrinsics are the same as $\Pi^{(0)}$ and map the partial video to the point cloud with the partial depths. We employ (7) to calculate the distance \bar{D} between a ray and the point cloud. We progressively add noise to the video \hat{I} to generate noisy

video z_τ where τ is the noise step. We employ ControlNet [59] to introduce the ray information into the video outpainting model. Let θ_v, θ_c denote the training parameters of the video diffusion model and ControlNet model. The training objective is

$$\mathcal{L} = \mathbb{E}_{z_0, \hat{I}, \tau, \hat{D}, \bar{D}, s, \epsilon} \|\epsilon - \epsilon_{\theta_v, \theta_c}(\hat{I}, z_\tau, \tau, \hat{D}, \bar{D}, s)\|_2^2, \quad (8)$$

where $\epsilon \sim \mathcal{N}(0, 1)$ is the diffusion noise. We train the outpainting model in an end-to-end manner.

3.3. Dynamic Scene Update

Now that we have an outpainted video $I^{(1)}$ at the new pose $\Pi^{(1)}$, the next step is to produce a new dynamic point cloud and merge it with the previous one $\mathcal{P}^{(0)}$.

Point cloud merging. We exploit the depth model [37] to obtain the video depth maps $D^{(1)}$ of the outpainted video $I^{(1)}$. Noting that there is a depth inconsistent problem between the estimated depths and the rendered ray depth map $\hat{D}^{(1)}$ in the mask regions $\hat{M}^{(1)}$, we follow common practices [57, 58] to align the video depth maps $D^{(1)}$ with the ray depth maps $\hat{D}^{(1)}$ by finetuning the depth estimation model. After obtaining the aligned depth maps from the finetuned depth model, we follow §3.1 to initialize foreground point cloud $\mathcal{P}^{(1,f)}$ and background point cloud

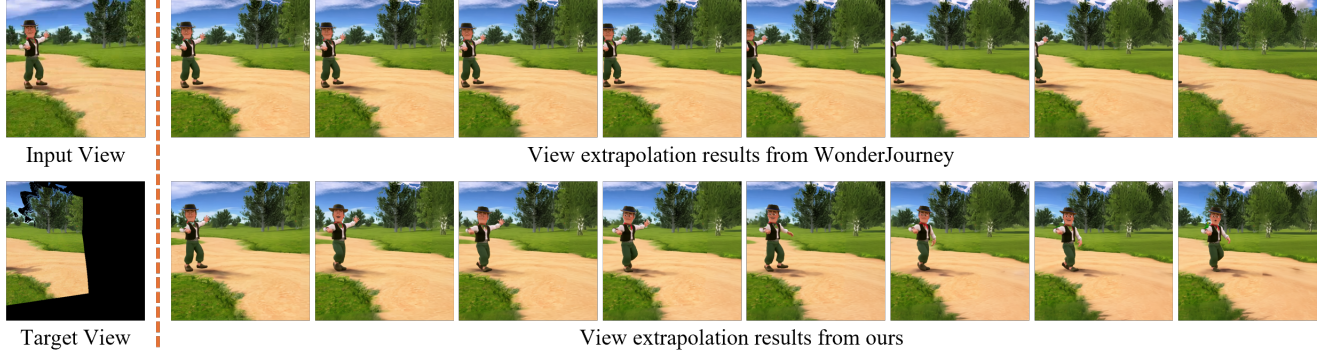


Figure 7. View extrapolation results. While Wonderjourney [58] only extrapolates views of a static character in 3D space, DynamicVoyager renders extrapolated views with 3D consistent motions by leveraging the ray information for scene outpainting.

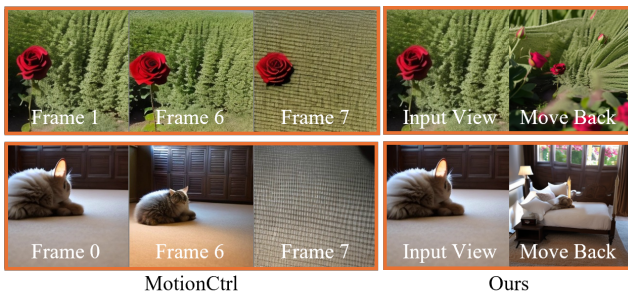


Figure 8. Visual comparisons with video diffusion model MotionCtrl [48]. Full details are in *supplementary material*. DynamicVoyager outpaints the scenes with large camera motions.

$\mathcal{P}^{(1,b)}$. Then we merge the new point clouds with the previous one to update the dynamic scenes,

$$\mathcal{P}^{(1)} = \mathcal{P}^{(1,f)} \cup \mathcal{P}^{(1,b)} \cup \mathcal{P}^{(0)}, \quad (9)$$

where $\mathcal{P}^{(1)}$ is the updated point cloud at the pose $\mathbf{\Pi}^{(1)}$. In this way, we could generate unbounded dynamic scenes along fly-through camera trajectories by looping §3.2 and §3.3 with new camera poses and scene prompts.

Background completion. In practice, we find that the missing background point clouds occluded by the moving foreground in the scene cause inconsistency when rendering along fly-through camera trajectories (as shown in Figure 4). We hence propose to employ our video outpainting model to generate background videos of the occlusion parts. After that, we extract depth maps of the background videos and reconstruct the background point clouds with the extracted depth maps. Details are in *supplementary material*. We also update the scene with these point clouds.

4. Experiments

In this section, we first describe the details of our experiment setups. Then, we discuss the results of the scene

Table 1. Quantitative results of controllable dynamic scene generation on the dynamic degree (DD), factual consistency (FC) [14] and CLIP [36] scores. While WonderJourney [58] only controls static scene generation with scene prompts, our model achieves controllable dynamic scene generation with higher performance.

methods	WonderJourney [58]	ours
CLIP-SIM \uparrow / DD \uparrow / FC \uparrow	24.98 / 2.23 / 1.30	25.23 / 3.13 / 1.32

generation with fly-through cameras and controllable scene generation. We finally conduct ablation studies of our model.

4.1. Experiment Setups

Data. We trained our outpainting model with the OpenVid dataset [33], which contains high-resolution videos with detailed video prompts. In order to train with daily dynamic scene videos, we sampled 5×10^3 videos that contain outdoor dynamic scenes, including natural scenes (such as waterfalls, rivers and moving clouds) and urban scenes (such as walking people and moving cars). Further data curation details are in *supplementary material*.

Training details. For training the proposed video outpainting model, we employed the LoRA [18] strategy to finetune the CogvideoX-5B-I2V diffusion model [54] with ControlNet [59]. The LoRA rank was 256 and the learning rate was 1×10^{-4} with a cosine schedule. The video resolution is $16 \times 512 \times 512$ and hence $N = 16$ and $h = w = 512$. For calculating the ray information, we introduced the depth model [37] to extract the depth map of each video frame. Then we followed MOTIA [46] and exploited the same mask strategy to generate partial videos.

Camera details. To set up dynamic scenes with fly-through camera trajectories, we followed the common practices [23, 35, 58] to move cameras following a straight line or doing a rotation. For the straight line, we used 0.0005 camera speed to move backward. For camera rotation, the rotation

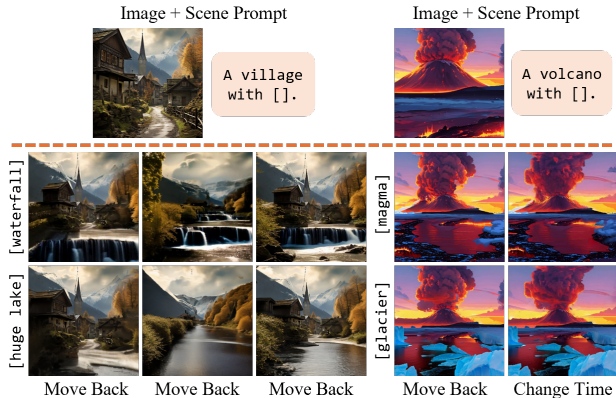


Figure 9. Controllable scene generation from input images with scene prompts. Full details are shown in *supplementary material*. DynamicVoyager successfully controls the dynamic scene outpainting content with the corresponding scene prompt.

radians were 0.45. We generated camera paths by linearly interpolating the translation and rotation between two camera poses. Along each path, we evenly sampled 16 views to synthesize fly-through videos.

4.2. Scene Generation with Fly-through Cameras

Figure 6 shows the dynamic scene generation results with long fly-through trajectories. We tested our model on both the background dynamics (water flowing in the waterfall) and the foreground dynamics (person walking on the path). Compared to the initial point cloud, our model generated unbounded dynamic scenes by exploiting the proposed scene outpainting process. As there is no direct baseline for unbounded dynamic scene generation, we compare our method with unbounded static scene generation method WonderJourney [58] in Figure 7, state-of-the-art 4D scene generation model CAT4D [49] in Figure 2 and camera-controllable video diffusion model MotionCtrl [48] in Figure 8. These figures demonstrate that our model can better generate unbounded dynamic scenes with 3D consistent motions by exploiting our ray outpainting model.

4.3. Scene Generation Controlled by Text

To test the controllable dynamic scene generation ability of our model, we generated dynamic scenes from village and volcano images with scene prompts. As shown in Figure 9, for the village image, we control the outpainting content by introducing two different text prompts: waterfall and huge lake. For the volcano image, we prompted the model to generate glacier and magma. It can be seen that our model successfully controls the unbounded dynamic scene generation with the given scene prompts. We followed the common practices [23, 56–58] to employ the CLIP [36] scores between the novel view images and the input scene

Table 2. Quantitative results of 3D consistent motions. VQ, TC and TA respectively denote the visual quality, temporal consistency and text-to-video alignment matrices [14]. Our model achieves better performance by achieving 3D consistent motions.

methods	CLIP-SIM \uparrow	VQ \uparrow	TC \uparrow	TA \uparrow	FC \uparrow
MOTIA [46]	23.80	2.281	1.852	2.656	1.859
w/o ray info	23.12	2.562	1.984	2.672	1.977
DynamicVoyager	24.70	2.578	2.234	2.938	2.188

Table 3. Quantitative ablation studies of the proposed foreground layer (§3.1) and background completion (§3.3) strategy.

methods	CLIP-SIM \uparrow	VQ \uparrow	TC \uparrow	TA \uparrow	FC \uparrow
w/o fg layer	23.88	1.891	0.871	2.219	1.102
w/o bg completion	24.62	1.906	0.871	2.547	1.195
DynamicVoyager	25.48	1.977	1.031	2.562	1.320

prompts and the dynamic degree (DD) and factual consistency (FC) indices proposed by VideoScore [14] to thoroughly evaluate the generation quality of the video. Table 1 shows that, while WonderJourney only generates static scenes with scene prompts, our model achieves better performance by controlling dynamic scene generation.

4.4. Ablation Study

Ray outpainting. To fairly evaluate the proposed ray outpainting model, we conducted experiments on five scenes containing common dynamic objects: cars, people, water and clouds. For each scene, we sampled 16 novel view images from the generated dynamic point cloud at 16 different timestamps along the fly-through camera trajectories. As there is no 3D video outpainting model baselines, we chose 2D outpainting model MOTIA [46] for comparisons. Figure 5 shows that by introducing the ray information for outpainting, our model successfully outpaints 3D consistent motions at the outpainting boundaries. In this way, our ray outpainting model achieves better performance in Table 2.

4D representation. We tested the proposed foreground representation and background completion strategy in Figure 4 and Table 3. It can be seen that our model renders consistent foregrounds with foreground layers and generates a plausible background with the background completion strategy.

5. Conclusion

In this paper, we propose DynamicVoyager to voyage into unbounded dynamic scenes from a single view. We reformulate dynamic scene generation as an outpainting problem. We consider pixels as rays to outpaint dynamic scenes with the ray context for 3D consistent motions. Experiments demonstrate that our model can generate unbounded dynamic scenes with consistent motions and control the

generated contents with scene prompts.

Limitations. Handling reflections, shadow segmentations (shadows of the cartoon man are considered as backgrounds), smaller structure segmentations, full multiview object rendering, complex motions and depth disconnection are exciting future directions.

Acknowledgments. We sincerely thank Prof. Kostas Daniilidis, Dr. Jiahui Lei, Qiao Feng, Chen Wang, and Uday Kiran for their generous and insightful feedback on this work.

References

- [1] Sherwin Bahmani, Ivan Skorokhodov, Aliaksandr Siarohin, Willi Menapace, Guocheng Qian, Michael Vasilkovsky, Hsin-Ying Lee, Chaoyang Wang, Jiayu Zou, Andrea Tagliasacchi, et al. VD3D: Taming large video diffusion transformers for 3D camera control. In *ICLR*, 2025. 3
- [2] Miguel Angel Bautista, Pengsheng Guo, Samira Abnar, Walter Talbott, Alexander Toshev, Zhuoyuan Chen, Laurent Dinh, Shuangfei Zhai, Hanlin Goh, Daniel Ulbricht, et al. Gaudi: A neural architect for immersive 3D scene generation. In *NeurIPS*, 2022. 2
- [3] Andreas Blattmann, Tim Dockhorn, Sumith Kulal, Daniel Mendelevitch, Maciej Kilian, Dominik Lorenz, Yam Levi, Zion English, Vikram Voleti, Adam Letts, et al. Stable video diffusion: Scaling latent video diffusion models to large datasets. *arXiv preprint arXiv:2311.15127*, 2023. 2
- [4] Michael Broxton, John Flynn, Ryan Overbeck, Daniel Erickson, Peter Hedman, Matthew Duvall, Jason Dourgarian, Jay Busch, Matt Whalen, and Paul Debevec. Immersive light field video with a layered mesh representation. In *ToG*, 2020. 2
- [5] Alvaro Collet, Ming Chuang, Pat Sweeney, Don Gillett, Dennis Evseev, David Calabrese, Hugues Hoppe, Adam Kirk, and Steve Sullivan. High-quality streamable free-viewpoint video. In *ToG*, 2015. 2
- [6] Matt Deitke, Dustin Schwenk, Jordi Salvador, Luca Weihs, Oscar Michel, Eli VanderBilt, Ludwig Schmidt, Kiana Ehsani, Aniruddha Kembhavi, and Ali Farhadi. Objaverse: A universe of annotated 3d objects. In *CVPR*, 2023. 3
- [7] Terrance DeVries, Miguel Angel Bautista, Nitish Srivastava, Graham W Taylor, and Joshua M Susskind. Unconstrained scene generation with locally conditioned radiance fields. In *ICCV*, 2021. 2
- [8] Rafail Fridman, Amit Abecasis, Yoni Kasten, and Tali Dekel. SceneScape: Text-driven consistent scene generation. In *NeurIPS*, 2023. 2
- [9] C Gan, J Schwartz, S Alter, M Schrimpf, J Traer, J De Freitas, J Kubilius, A Bhandwadar, N Haber, M Sano, et al. ThreeDWorld: A platform for interactive multi-modal physical simulation. In *NeurIPS*, 2021. 2
- [10] Ruiqi Gao*, Aleksander Holynski*, Philipp Henzler, Arthur Brussee, Ricardo Martin-Brualla, Pratul P. Srinivasan, Jonathan T. Barron, and Ben Poole*. CAT3D: Create anything in 3D with multi-view diffusion models. In *NeurIPS*, 2024. 2
- [11] Jiayuan Gu, Fanbo Xiang, Xuanlin Li, Zhan Ling, Xiqiang Liu, Tongzhou Mu, Yihe Tang, Stone Tao, Xinyue Wei, Yunchao Yao, Xiaodi Yuan, Pengwei Xie, Zhiao Huang, Rui Chen, and Hao Su. ManiSkill2: A unified benchmark for generalizable manipulation skills. In *ICLR*, 2023. 2
- [12] Yuwei Guo, Ceyuan Yang, Anyi Rao, Zhengyang Liang, Yaohui Wang, Yu Qiao, Maneesh Agrawala, Dahua Lin, and Bo Dai. AnimateDiff: Animate your personalized text-to-image diffusion models without specific tuning. In *ICLR*, 2024. 3
- [13] Hao He, Yinghao Xu, Yuwei Guo, Gordon Wetzstein, Bo Dai, Hongsheng Li, and Ceyuan Yang. CameraCtrl: Enabling camera control for text-to-video generation. In *ICLR*, 2025. 3
- [14] Xuan He, Dongfu Jiang, Ge Zhang, Max Ku, Achint Soni, Sherman Siu, Haonan Chen, Abhuranil Chandra, Ziyan Jiang, Aaran Arulraj, Kai Wang, Quy Duc Do, Yuansheng Ni, Bohan Lyu, Yaswanth Narsupalli, Rongqi Fan, Zhiheng Lyu, Yuchen Lin, and Wenhui Chen. VideoScore: Building automatic metrics to simulate fine-grained human feedback for video generation. In *EMNLP*, 2024. 7, 8
- [15] Lukas Höllein, Ang Cao, Andrew Owens, Justin Johnson, and Matthias Nießner. Text2Room: Extracting textured 3D meshes from 2D text-to-image models. In *ICCV*, 2023. 2
- [16] Wenyi Hong, Ming Ding, Wendi Zheng, Xinghan Liu, and Jie Tang. CogVideo: Large-scale pretraining for text-to-video generation via transformers. In *ICLR*, 2022. 2, 3
- [17] Chen Hou, Guoqiang Wei, Yan Zeng, and Zhibo Chen. Training-free camera control for video generation. In *ICLR*, 2025. 1, 3
- [18] Edward J Hu, Yelong Shen, Phillip Wallis, Zeyuan Allen-Zhu, Yuanzhi Li, Shean Wang, Lu Wang, Weizhu Chen, et al. LoRA: Low-rank adaptation of large language models. In *ICLR*, 2022. 7
- [19] Ronghang Hu, Nikhila Ravi, Alexander C Berg, and Deepak Pathak. Worldsheet: Wrapping the world in a 3d sheet for view synthesis from a single image. In *ICCV*, 2021. 2
- [20] Jitesh Jain, Jiachen Li, Mang Tik Chiu, Ali Hassani, Nikita Orlov, and Humphrey Shi. OneFormer: One transformer to rule universal image segmentation. In *CVPR*, 2023. 2, 3, 4
- [21] Bernhard Kerbl, Georgios Kopanas, Thomas Leimkühler, and George Drettakis. 3D gaussian splatting for real-time radiance field rendering. In *TOG*, 2023. 2
- [22] Alexander Kirillov, Eric Mintun, Nikhila Ravi, Hanzi Mao, Chloe Rolland, Laura Gustafson, Tete Xiao, Spencer Whitehead, Alexander C Berg, Wan-Yen Lo, et al. Segment anything. In *ICCV*, 2023. 2, 3, 12
- [23] Hanyang Kong, Dongze Lian, Michael Bi Mi, and Xinchao Wang. DreamDrone: Text-to-image diffusion models are zero-shot perpetual view generators. In *ECCV*, 2024. 5, 7, 8
- [24] Zhengfei Kuang, Shengqu Cai, Hao He, Yinghao Xu, Hongsheng Li, Leonidas Guibas, and Gordon Wetzstein. Collaborative video diffusion: Consistent multi-video generation with camera control. In *NeurIPS*, 2024. 3
- [25] Jiabao Lei, Jiapeng Tang, and Kui Jia. RGBD2: Generative scene synthesis via incremental view inpainting using RGBD diffusion models. In *CVPR*, 2023. 2

- [26] Renjie Li, Panwang Pan, Bangbang Yang, Dejia Xu, Shijie Zhou, Xuanyang Zhang, Zeming Li, Achuta Kadambi, Zhangyang Wang, Zhengzhong Tu, et al. 4K4DGen: Panoramic 4D generation at 4K resolution. In *ICLR*, 2025. 2, 3
- [27] Zhengqi Li, Qianqian Wang, Noah Snavely, and Angjoo Kanazawa. Infinitenature-Zero: Learning perpetual view generation of natural scenes from single images. In *ECCV*, 2022. 2
- [28] Huan Ling, Seung Wook Kim, Antonio Torralba, Sanja Fidler, and Karsten Kreis. Align your gaussians: Text-to-4D with dynamic 3D gaussians and composed diffusion models. In *CVPR*, 2024. 2, 3
- [29] Lu Ling, Yichen Sheng, Zhi Tu, Wentian Zhao, Cheng Xin, Kun Wan, Lantao Yu, Qianyu Guo, Zixun Yu, Yawen Lu, et al. DL3DV-10K: A large-scale scene dataset for deep learning-based 3D vision. In *CVPR*, 2024. 3
- [30] Andrew Liu, Richard Tucker, Varun Jampani, Ameesh Makadia, Noah Snavely, and Angjoo Kanazawa. Infinite Nature: Perpetual view generation of natural scenes from a single image. In *ICCV*, 2021. 2
- [31] Yuan Liu, Cheng Lin, Zijiao Zeng, Xiaoxiao Long, Lingjie Liu, Taku Komura, and Wenping Wang. SyncDreamer: Generating multiview-consistent images from a single-view image. In *ICLR*, 2024. 1, 2
- [32] Ben Mildenhall, Pratul P. Srinivasan, Matthew Tancik, Jonathan T. Barron, Ravi Ramamoorthi, and Ren Ng. NeRF: Representing scenes as neural radiance fields for view synthesis. In *ECCV*, 2020. 2
- [33] Kepan Nan, Rui Xie, Penghao Zhou, Tiehan Fan, Zhenheng Yang, Zhijie Chen, Xiang Li, Jian Yang, and Ying Tai. Openvid-1M: A large-scale high-quality dataset for text-to-video generation. In *ICLR*, 2025. 7, 12
- [34] Zijie Pan, Zeyu Yang, Xiatian Zhu, and Li Zhang. Efficient4D: Fast dynamic 3D object generation from a single-view video. *arXiv preprint arXiv:2401.08742*, 2024. 3
- [35] Stefan Popov, Amit Raj, Michael Krainin, Yuanzhen Li, William T. Freeman, and Michael Rubinstein. CamCtrl3D: Single-image scene exploration with precise 3D camera control. In *3DV*, 2025. 2, 7
- [36] Alec Radford, Jong Wook Kim, Chris Hallacy, Aditya Ramesh, Gabriel Goh, Sandhini Agarwal, Girish Sastry, Amanda Askell, Pamela Mishkin, Jack Clark, et al. Learning transferable visual models from natural language supervision. In *ICML*, 2021. 7, 8
- [37] René Ranftl, Katrin Lasinger, David Hafner, Konrad Schindler, and Vladlen Koltun. Towards robust monocular depth estimation: Mixing datasets for zero-shot cross-dataset transfer. In *IEEE TPAMI*, 2020. 2, 3, 4, 6, 7, 12
- [38] Jiawei Ren, Liang Pan, Jiaxiang Tang, Chi Zhang, Ang Cao, Gang Zeng, and Ziwei Liu. DreamGaussian4D: Generative 4D gaussian splatting. *arXiv preprint arXiv:2312.17142*, 2023. 3
- [39] Xuanchi Ren, Tianchang Shen, Jiahui Huang, Huan Ling, Yifan Lu, Merlin Nimier-David, Thomas Müller, Alexander Keller, Sanja Fidler, and Jun Gao. GEN3C: 3d-informed world-consistent video generation with precise camera control. In *CVPR*, 2025. 3
- [40] Robin Rombach, Andreas Blattmann, Dominik Lorenz, Patrick Esser, and Björn Ommer. High-resolution image synthesis with latent diffusion models. In *CVPR*, 2022. 2
- [41] Jiaming Song, Chenlin Meng, and Stefano Ermon. Denoising diffusion implicit models. In *ICLR*, 2021. 2
- [42] Wenqiang Sun, Shuo Chen, Fangfu Liu, Zilong Chen, Yueqi Duan, Jun Zhang, and Yikai Wang. DimensionX: Create any 3D and 4D scenes from a single image with controllable video diffusion. *arXiv preprint arXiv:2411.04928*, 2024. 2, 3
- [43] Fengrui Tian, Shaoyi Du, and Yueqi Duan. MonoNeRF: Learning a generalizable dynamic radiance field from monocular videos. In *ICCV*, 2023. 2
- [44] Fengrui Tian, Yueqi Duan, Angtian Wang, Jianfei Guo, and Shaoyi Du. Semantic Flow: Learning semantic fields of dynamic scenes from monocular videos. In *ICLR*, 2024. 2
- [45] Basile Van Hoorick, Rundi Wu, Ege Ozguroglu, Kyle Sargent, Ruoshi Liu, Pavel Tokmakov, Achal Dave, Changxi Zheng, and Carl Vondrick. Generative camera dolly: Extreme monocular dynamic novel view synthesis. In *ECCV*, 2024. 3
- [46] Fu-Yun Wang, Xiaoshi Wu, Zhaoyang Huang, Xiaoyu Shi, Dazhong Shen, Guanglu Song, Yu Liu, and Hongsheng Li. Be-your-outpainter: Mastering video outpainting through input-specific adaptation. In *ECCV*, 2024. 5, 7, 8
- [47] Shuzhe Wang, Vincent Leroy, Yohann Cabon, Boris Chidlovskii, and Jerome Revaud. DUST3R: Geometric 3D vision made easy. In *CVPR*, 2024. 2
- [48] Zhouxia Wang, Ziyang Yuan, Xintao Wang, Yaowei Li, Tianshui Chen, Menghan Xia, Ping Luo, and Ying Shan. Motionctrl: A unified and flexible motion controller for video generation. In *ACM SIGGRAPH*, 2023. 7, 8, 12, 15
- [49] Rundi Wu, Ruiqi Gao, Ben Poole, Alex Trevithick, Changxi Zheng, Jonathan T Barron, and Aleksander Holynski. Cat4D: Create anything in 4D with multi-view video diffusion models. *arXiv preprint arXiv:2411.18613*, 2024. 2, 3, 8
- [50] Yiming Xie, Chun-Han Yao, Vikram Voleti, Huaizu Jiang, and Varun Jampani. SV4D: Dynamic 3D content generation with multi-frame and multi-view consistency. *arXiv preprint arXiv:2407.17470*, 2024. 2, 3
- [51] Jinbo Xing, Menghan Xia, Yong Zhang, Haoxin Chen, Wangbo Yu, Hanyuan Liu, Gongye Liu, Xintao Wang, Ying Shan, and Tien-Tsin Wong. Dynamicrafter: Animating open-domain images with video diffusion priors. In *ICLR*, 2024. 3
- [52] Jihan Yang, Shusheng Yang, Anjali W. Gupta, Rilyn Han, Li Fei-Fei, and Saining Xie. Thinking in Space: How multimodal large language models see, remember and recall spaces. *arXiv preprint arXiv:2412.14171*, 2024. 2
- [53] Shiyuan Yang, Liang Hou, Haibin Huang, Chongyang Ma, Pengfei Wan, Di Zhang, Xiaodong Chen, and Jing Liao. Direct-a-Video: Customized video generation with user-directed camera movement and object motion. In *SIGGRAPH*, 2024. 3
- [54] Zhuoyi Yang, Jiayan Teng, Wendi Zheng, Ming Ding, Shiyu Huang, Jiazheng Xu, Yuanming Yang, Wenyi Hong, Xiaohan Zhang, Guanyu Feng, et al. CogVideoX: Text-to-video

- diffusion models with an expert transformer. In *ICLR*, 2024. [2](#), [3](#), [4](#), [7](#)
- [55] Yuyang Yin, Dejia Xu, Zhangyang Wang, Yao Zhao, and Yunchao Wei. 4DGen: Grounded 4D content generation with spatial-temporal consistency. *arXiv preprint arXiv:2312.17225*, 2023. [3](#)
- [56] Heng Yu, Chaoyang Wang, Peiye Zhuang, Willi Menapace, Aliaksandr Siarohin, Junli Cao, Laszlo A Jeni, Sergey Tulyakov, and Hsin-Ying Lee. 4Real: Towards photorealistic 4D scene generation via video diffusion models. In *NeurIPS*, 2024. [2](#), [3](#), [8](#)
- [57] Hong-Xing Yu, Haoyi Duan, Charles Herrmann, William T Freeman, and Jiajun Wu. WonderWorld: Interactive 3D scene generation from a single image. *arXiv preprint arXiv:2406.09394*, 2024. [1](#), [2](#), [5](#), [6](#)
- [58] Hong-Xing Yu, Haoyi Duan, Junhwa Hur, Kyle Sargent, Michael Rubinstein, William T Freeman, Forrester Cole, Deqing Sun, Noah Snavely, Jiajun Wu, et al. WonderJourney: Going from anywhere to everywhere. In *CVPR*, 2024. [1](#), [2](#), [5](#), [6](#), [7](#), [8](#), [12](#), [14](#)
- [59] Lvmin Zhang, Anyi Rao, and Maneesh Agrawala. Adding conditional control to text-to-image diffusion models. In *ICCV*, 2023. [6](#), [7](#)
- [60] Yuyang Zhao, Chung-Ching Lin, Kevin Lin, Zhiwen Yan, Linjie Li, Zhengyuan Yang, Jianfeng Wang, Gim Hee Lee, and Lijuan Wang. GenXD: Generating any 3D and 4D scenes. In *ICLR*, 2025. [3](#)

We organize the supplementary material as follows.

- §6 provides an additional video for better visualization of the generated dynamic scenes, implementation code of DynamicVoyager, and a table of notations used in the paper.
- §7 presents more implementation details of the proposed ray outpainting model and 4D point cloud reconstruction.
- §8 introduces the details of the background completion strategy.
- §9 presents more scene generation results and details of camera-controllable video diffusion model MotionCtrl [48].

6. Video, Code, and Notation Table

We encourage readers to watch the video in the supplementary material to better understand our visualization results. Moreover, we provide the implementation code in the supplementary material; our code and pretrained models will be publicly available. For convenience, we summarize the notations in the paper in Table 4.

7. Implementation Details

We present further implementation details and the dataset filtering process here.

Scene generation details. Inspired by WonderJourney [58], we adjust the depth maps with SAM [22] to promote spatio-temporal consistency of the depth for each object in the scene.

Dataset filtering process. We used the keywords in Table 5 to filter videos in OpenVid [33]. After filtering, we randomly selected 5×10^3 videos to fine-tune our video outpainting models.

8. Background Completion

As described in the method section of the main paper, in practice, we find that background regions occluded by the dynamic foregrounds can become exposed when rendering the dynamic scene with a fly-through camera trajectory. Since these regions are fully occluded by the foregrounds under camera pose $\Pi^{(i)}$, the missing parts cause inconsistent colors in 3D when rendering the dynamic scene with fly-through cameras. To address this issue, we propose to employ our outpainting model to fill the missing colors in the background. More specifically, after obtaining the fixed viewpoint video $I^{(i)}$, the depth maps $D^{(i)}$ and foreground masks $M^{(i)}$, we obtain the background video $I^{(i,b)}$ by employing foreground masks on the video $I^{(i)}$. For the regions occluded by the foreground in the video $I^{(i,b)}$, we sample the ray information following (5), (6) and (7) in the main paper. Then we exploit our ray outpainting model to inpaint the video colors at the occluded regions with the sampled ray information. After that, we obtain the background depths of these regions with a depth estimation model [37]

and reconstruct the background point cloud on these regions. Finally, we merge these occluded background point clouds into our dynamic scene point cloud.

9. More Dynamic Scene Generation Results

Space-time interpolation. Figure 10 presents visualizations of space-time interpolation results. In this figure, a cartoon cat is playing guitar with moving clouds. It can be seen that our model successfully renders dynamic scenes with fly-through cameras, while WonderJourney [58] only interpolates in the static scene.

Controllable scene generation. Figure 11 reports additional results on controllable scene generation. We control the village scene to generate cascade waterfall and huge lake separately. It can be seen that our model successfully controls scene generations with fly-through cameras.

MotionCtrl comparison details. We chose to compare with MotionCtrl [48], which is a camera-controllable video diffusion model presented in the figure of the main paper. As MotionCtrl only generates videos from text prompts, we use the first frame generated by MotionCtrl as the input of our model. To test the camera control performance in the MotionCtrl model, we evenly sample 16 camera translations from $[0, 0, 0]$ to $[0, 0, 40]$ and introduce them into MotionCtrl models. The results are shown in Figure 12. As MotionCtrl learns from training videos with relatively limited camera movements, it fails to generate videos with large camera motions.

Table 4. Notations.

Notation	Description
$\Pi^{(i)}$	Camera pose for the i^{th} view
$I^{(i)}$	Video frames at pose $\Pi^{(i)}$: $\{I_t^{(i)} \in \mathbb{R}^{h \times w \times 3}\}_{t=0}^{N-1}$
$I_t^{(i)}$	Video frame at timestamp t and pose $\Pi^{(i)}$
$D^{(i)}$	Depth maps at pose $\Pi^{(i)}$: $\{D_t^{(i)} \in \mathbb{R}^{h \times w}\}_{t=0}^{N-1}$
$D_t^{(i)}$	Depth map at timestamp t and pose $\Pi^{(i)}$
$M^{(i)}$	Binary foreground masks at pose $\Pi^{(i)}$: $\{M_t^{(i)} \in \{0, 1\}^{h \times w}\}_{t=0}^{N-1}$
$M_t^{(i)}$	Binary foreground mask at timestamp t and pose $\Pi^{(i)}$
$\mathcal{P}^{(i)}$	4D point cloud constructed until pose $\Pi^{(i)}$
$\mathcal{P}_t^{(i)}$	4D point cloud at timestamp t constructed until pose $\Pi^{(i)}$
\mathbf{p}	Point in 4D point cloud: $\mathbf{p} = (\mathbf{x}, t, \mathbf{c})$ with position \mathbf{x} , timestamp t , color \mathbf{c}
\mathbf{x}	3D position of a point, $\mathbf{x} \in \mathbb{R}^3$
\mathbf{c}	Color of a point, $\mathbf{c} \in \mathbb{R}^3$
$\mathcal{P}^{(i,f)}, \mathcal{P}^{(i,b)}$	Foreground, background point cloud until pose $\Pi^{(i)}$
$I^{(i,f)}, I^{(i,b)}$	Foreground, background video frames at pose $\Pi^{(i)}$
$D^{(i,f)}, D^{(i,b)}$	Foreground, background depth maps at pose $\Pi^{(i)}$
ϕ	Mapping function from 2D image and depth to 3D point cloud
φ	Image rasterization function
$\hat{I}^{(i)}$	Rasterized (partial) video at pose $\Pi^{(i)}$ given point cloud $\mathcal{P}^{(i-1)}$
$\hat{D}^{(i)}$	Rasterized ray depth maps at pose $\Pi^{(i)}$ given point cloud $\mathcal{P}^{(i-1)}$
$\hat{M}^{(i)}$	Binary masks for observed regions in rasterization at pose $\Pi^{(i)}$
$r^{(i)}(x, y)$	Unit-norm ray vector from camera origin at pose $\Pi^{(i)}$ to pixel (x, y)
$\mathbf{o}^{(i)}$	Camera center of pose $\Pi^{(i)}$
dist_{r2p}	Distance function between a ray and a point
$\bar{D}_t^{(i)}$	Distance map between rays and point cloud at timestamp t
\mathbf{s}	Scene prompt describing desired motion
z_τ	Noisy video at noise step τ
θ_v	Training parameters of video diffusion model
θ_c	Training parameters of ControlNet

Table 5. Filter keywords.

keywords	mountain, forest, river, lake, ocean, canyon, meadow, hill, city, trees, cloud, wind, nature grassland, beach, snow, waterfall, stream, wildlife, pond, dunes, island, rainforest, sunset, sunrise, storm, rain, thunderstorm snowstorm, lightning, rainbow, twilight, dawn, dusk, star, aurora, moon, downtown, skyline, street, road, pedestrians, crowd transport, bridge, tower, skyscraper, urban, bustling, bus, metropolis, coast, beachfront, harbor, port, pier, boat, yacht dock, marina, waterfront, seaside, swimming, surf, sailboat, sun, shore, tidal, waves, bay, lagoon, village, town, countryside rural, greenhouse, sunflower field, landscape, sky, lake, water, sea, seas, cityscape, pedestrian, pedestrians, cars, traffic, people
----------	---

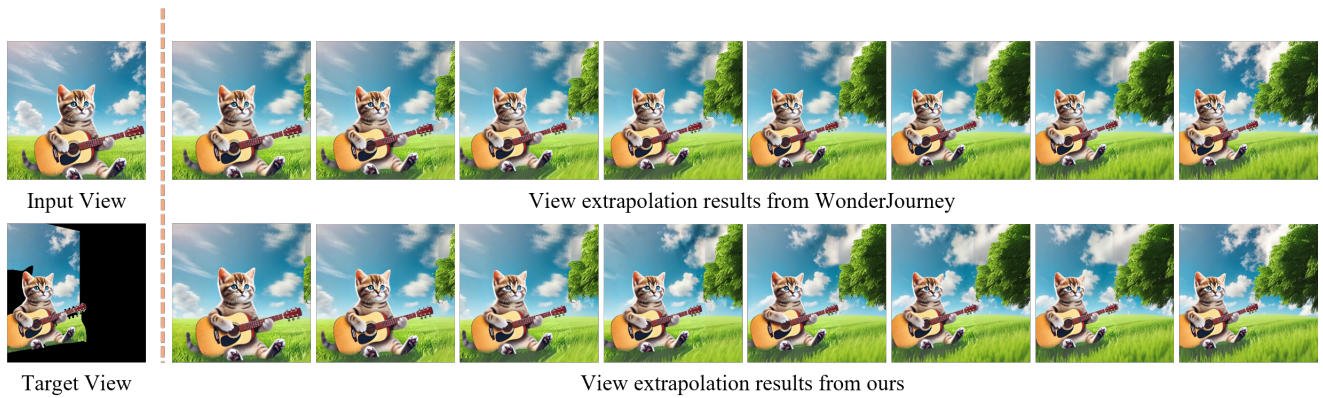


Figure 10. Space-time interpolation comparisons between DynamicVoyager and WonderJourney [58].

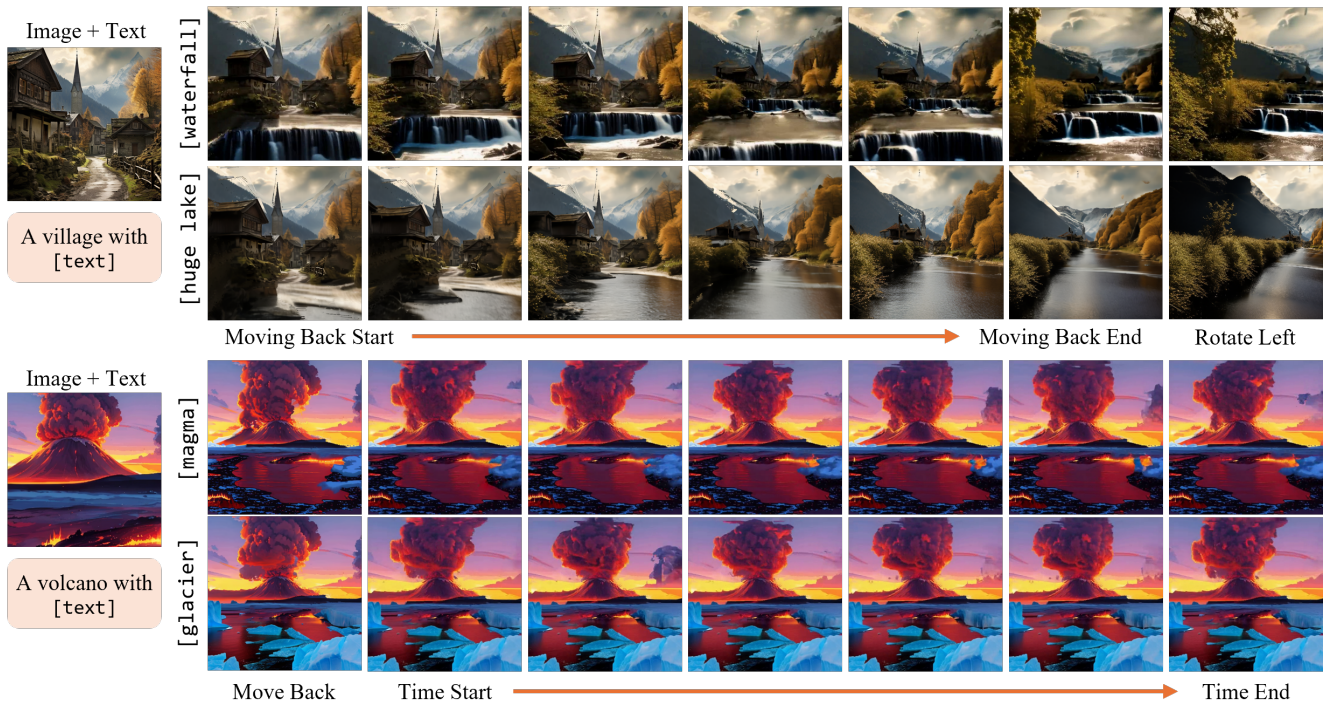
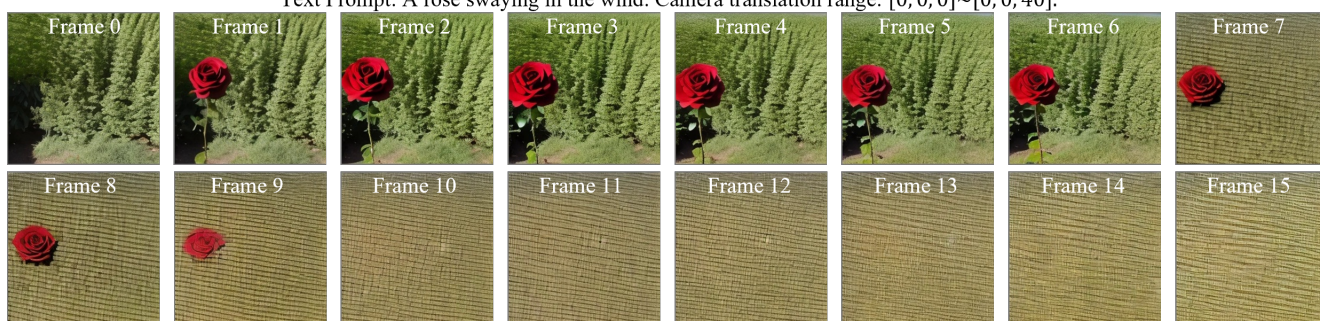


Figure 11. Controllable scene generation from input images with scene prompts. Given an image as input, DynamicVoyager successfully controls the dynamic scene outpainting content with the corresponding text prompt.

Text Prompt: A rose swaying in the wind. Camera translation range: $[0, 0, 0] \sim [0, 0, 40]$.



Text Prompt: A sleepy cat. Camera translation range: $[0, 0, 0] \sim [0, 0, 40]$.

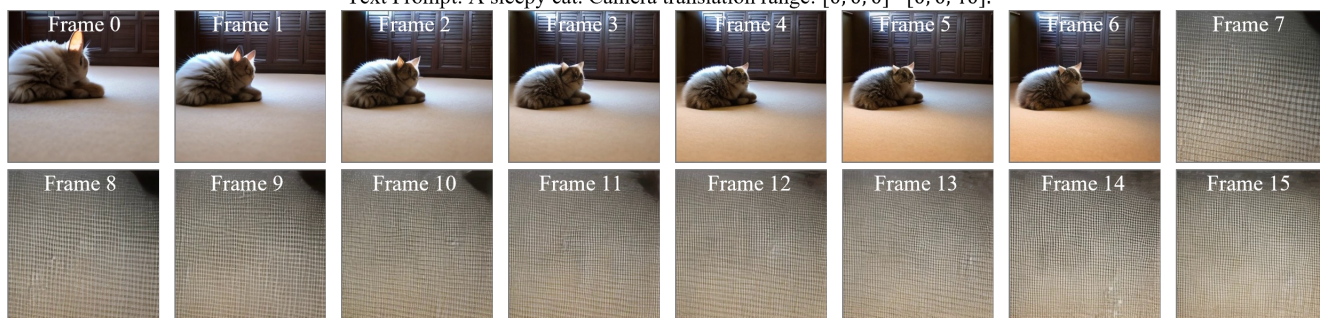


Figure 12. Detailed results of MotionCtrl [48] with large camera translation inputs. It can be seen that the model fails to generate videos with large camera motions.